

## **Implementation of quantum permutation algorithm with classical light**

### Author

Zhang, Shihao, Li, Pengyun, Wang, Bo, Zeng, Qiang, Zhang, Xiangdong

### Published

2019

### Journal Title

Journal of Physics Communications

### Version

Version of Record (VoR)

### DOI

[10.1088/2399-6528/aafc1c](https://doi.org/10.1088/2399-6528/aafc1c)

### Rights statement

© 2019 The Author(s). Published by IOP Publishing Ltd. Original content from this work may be used under the terms of the Creative Commons Attribution 3.0 licence. Any further distribution of this work must maintain attribution to the author(s) and the title of the work, journal citation and DOI.

### Downloaded from

<http://hdl.handle.net/10072/399841>

### Griffith Research Online

<https://research-repository.griffith.edu.au>

PAPER • OPEN ACCESS

## Implementation of quantum permutation algorithm with classical light

To cite this article: Shihao Zhang *et al* 2019 *J. Phys. Commun.* **3** 015008

View the [article online](#) for updates and enhancements.



## PAPER

## OPEN ACCESS

## RECEIVED

13 September 2018

## REVISED

7 December 2018

## ACCEPTED FOR PUBLICATION

4 January 2019

## PUBLISHED

22 January 2019

Original content from this work may be used under the terms of the [Creative Commons Attribution 3.0 licence](#).

Any further distribution of this work must maintain attribution to the author(s) and the title of the work, journal citation and DOI.



# Implementation of quantum permutation algorithm with classical light

Shihao Zhang<sup>1</sup> , Pengyun Li<sup>1,2</sup>, Bo Wang<sup>1</sup>, Qiang Zeng<sup>1</sup> and Xiangdong Zhang<sup>1</sup> <sup>1</sup> Beijing Key Laboratory of Nanophotonics & Ultrafine Optoelectronic Systems, School of Physics, Beijing Institute of Technology, 100081, Beijing, People's Republic of China<sup>2</sup> China Academy of Electronics and Information Technology, China Electronics Technology Group Corporation, Beijing 100041, People's Republic of ChinaE-mail: [zhangxd@bit.edu.cn](mailto:zhangxd@bit.edu.cn)**Keywords:** quantum permutation algorithm, classical light, orbital angular momentum, polarization

## Abstract

We report the experimental implementation of quantum permutation algorithm using polarization and orbital angular momentum of the classical optical beam. The easy-handling optical setup to realize all eight cyclic permutation transformations for an input four-dimensional system has been constructed. The two-to-one speed-up ratio to determine the parity of each permutation has been demonstrated. Moreover, we have theoretically discussed the extension to the case with eight elements, and the limitations on the generalization of our proposal to higher-dimensional cases. Our scheme exhibits outstanding stability and demonstrates that optical quantum computation is possible using classical states of light.

## 1. Introduction

In the past decades, the subject of quantum computation has attracted widespread interest both in the fields of theoretical quantum physics [1] and computer science [2] due to its potential computational power. A parallel development has also been achieved in experimental progress [3] and led to the impressive implementations of a variety of well-designed quantum algorithms, such as the Deutsch's algorithm for dealing with a black box problem [4, 5], Grover's search algorithm [6, 7], Shor's algorithm for integer factorization [8, 9], and the algorithm for solving systems of linear equations proposed by Harrow *et al* [10, 11].

Due to the delicate nature of quantum systems and the difficulties in implementing qualified unitary transforms and measurement, constructing a potentially scalable quantum computer or simulator with useful long coherence times still remains challenging [12]. Interestingly, by exploring certain common properties that photons and classical coherent light share (e.g. superposition, interference and correlation), researchers have exhibited a range of phenomena closely related to quantum behaviors [13–15] based on alternative classical wave-optics. As for the practical applications, one or multiple degrees of freedom (DOFs) of classical light have been exploited to demonstrate several typical quantum information processing tasks, such as the Deutsch-Jozsa algorithm [16, 17], quantum walk [18, 19] and Grover's algorithm [20, 21]. Besides, other classical systems have also been proposed similarly to emulate quantum computing, e.g., with analog electronic circuit devices [22, 23]. These classical schemes own advantages of relative ease of design and operations, and robustness to external perturbations over their quantum counterparts.

In recent years, a quantum speed-up algorithm called the quantum permutation algorithm has received concentration and been reported in quantum experimental implementations, including the NMR [24, 25], superconducting [26, 27] and linear optical systems [28, 29]. By contrast, this algorithm can also be demonstrated in the orbital angular momentum (OAM) space of classical light [30]. Inspired by this thought, in this work we explore how to realize the quantum permutation algorithm with the OAM and polarization DOFs of the classical light beams. In our proposal, the preparation of initial states, realization of all eight cyclic

permutation operations, and detection of final output states can all be conveniently accomplished via regular optical elements, and then we discuss its generalization to higher-dimensional cases theoretically.

## 2. Quantum permutation algorithm

Firstly, we give a brief description of the quantum permutation algorithm proposed by Gedik [25]. For a given set  $S$  with  $d$  elements denoted as  $S = \{1, 2, \dots, d-1, d\}$ ,  $2d$  different cyclic permutation operations performed by a black box acting on  $S$  can be classified into two categories. Specifically speaking, we call those  $d$  cyclic permutations  $f_1, f_2, \dots, f_d$  which map the set  $S$  to  $\{1, 2, \dots, d-1, d\}, \{2, 3, \dots, d, 1\}, \dots, \{d, 1, \dots, d-2, d-1\}$  respectively own positive parity, while the parity of other  $d$  cyclic permutations  $f_{d+1}, f_{d+2}, \dots, f_{2d}$  which separately map  $S$  to  $\{d, d-1, \dots, 2, 1\}, \{d-1, d-2, \dots, 1, d\}, \dots, \{1, d, \dots, 3, 2\}$  would be negative.

For example, the four positive cyclic permutations for  $d = 4$  can be expressed as

$$\begin{aligned} f_1 &= \begin{pmatrix} 1 & 2 & 3 & 4 \\ 1 & 2 & 3 & 4 \end{pmatrix}, f_2 = \begin{pmatrix} 1 & 2 & 3 & 4 \\ 2 & 3 & 4 & 1 \end{pmatrix}, \\ f_3 &= \begin{pmatrix} 1 & 2 & 3 & 4 \\ 3 & 4 & 1 & 2 \end{pmatrix}, f_4 = \begin{pmatrix} 1 & 2 & 3 & 4 \\ 4 & 1 & 2 & 3 \end{pmatrix} \end{aligned} \quad (1)$$

and the four negative cyclic permutations are

$$\begin{aligned} f_5 &= \begin{pmatrix} 1 & 2 & 3 & 4 \\ 4 & 3 & 2 & 1 \end{pmatrix}, f_6 = \begin{pmatrix} 1 & 2 & 3 & 4 \\ 3 & 2 & 1 & 4 \end{pmatrix}, \\ f_7 &= \begin{pmatrix} 1 & 2 & 3 & 4 \\ 2 & 1 & 4 & 3 \end{pmatrix}, f_8 = \begin{pmatrix} 1 & 2 & 3 & 4 \\ 1 & 4 & 3 & 2 \end{pmatrix} \end{aligned} \quad (2)$$

The question is how to determine the parity of a cyclic permutation in the black box. It can be observed from equations (1) and (2) that in the classical case one needs to run the permutation operation in the black box at least twice for different inputs. By comparison, the quantum permutation algorithm proposed by Gedik *et al* only needs one query to the black box to solve this problem.

When four state vectors  $|1\rangle = (1, 0, 0, 0)^T$ ,  $|2\rangle = (0, 1, 0, 0)^T$ ,  $|3\rangle = (0, 0, 1, 0)^T$ , and  $|4\rangle = (0, 0, 0, 1)^T$  are employed to represent the four elements  $\{1, 2, 3, 4\}$  in the set  $S$ , we can then consider an input state in the superposition of these four states

$$|\psi_{in}\rangle = |\psi_2\rangle = (|1\rangle + i|2\rangle - |3\rangle - i|4\rangle)/2 = (1, i, -1, -i)^T/2, \quad (3)$$

and refer to one of its orthogonal state as

$$|\psi_4\rangle = (|1\rangle - i|2\rangle - |3\rangle + i|4\rangle)/2 = (1, -i, -1, i)^T/2 \quad (4)$$

It can be easily verified that four positive cyclic operations  $\{f_1, f_2, f_3, f_4\}$  map the input state  $|\psi_{in}\rangle$  onto  $\{|\psi_2\rangle, -i|\psi_2\rangle, -|\psi_2\rangle, i|\psi_2\rangle\}$ , while the four negative cyclic operations  $\{f_5, f_6, f_7, f_8\}$  result in the outcomes  $\{-i|\psi_4\rangle, -|\psi_4\rangle, i|\psi_4\rangle, |\psi_4\rangle\}$ , respectively. Therefore, identifying the output states enables us to distinguish the parity of corresponding cyclic permutations.

Considering the analogy between the single photons and coherent states prepared in the same light modes, the implementation of the above quantum permutation algorithm can also be accomplished with classical light. For instance, the Laguerre–Gaussian modes of classical optical beams we exploit here are OAM eigenstates and solutions of the paraxial wave equation in cylindrical coordinates [31, 32]. Thus, OAM and polarization can be chosen as two proper DOFs to encode the four basis states of one *ququart*, and we particularly describe them by a slightly modified version of the bra-ket notation of quantum states for clarity as [33]

$$|+1, H\rangle \rightarrow |1\rangle, |+1, V\rangle \rightarrow |2\rangle, |-1, H\rangle \rightarrow |3\rangle, |-1, V\rangle \rightarrow |4\rangle \quad (5)$$

where the number  $+1$  and  $-1$  stand for two OAM modes (distinguished by the azimuthal index  $\ell$ ), while  $H$  and  $V$  for horizontal and vertical polarizations, respectively. Since this four-dimensional state space is spanned by the tensor product of Hilbert spaces of OAM and polarization, the encoded input state  $|\psi_{in}\rangle$  corresponding to equation (3) can be derived in a separable form as

$$\begin{aligned} |\psi_{in}\rangle &= |\psi_2\rangle = (|+1\rangle - |-1\rangle)(|H\rangle + i|V\rangle)/2 \\ &= (|+1\rangle - |-1\rangle)|L\rangle/\sqrt{2} \end{aligned} \quad (6)$$

**Table 1.** Implementations and output states of eight different permutation transformations for the case with  $d = 4$ . The mark  $\checkmark$  or  $\times$  means to add or remove the corresponding half-wave plate (HWP) at  $45^\circ$  and Dove prisms at  $0^\circ$  (DP<sub>1</sub>, DP<sub>2</sub>) in the black box.

Permutation operation	HWP	DP <sub>1</sub>	DP <sub>2</sub>	Parity	Output
$f_1$	$\times$	$\checkmark$	$\checkmark$	positive	$ \psi_2\rangle$
$f_2$	$\checkmark$	$\checkmark$	$\times$	positive	$-i \psi_2\rangle$
$f_3$	$\times$	$\times$	$\times$	positive	$- \psi_2\rangle$
$f_4$	$\checkmark$	$\times$	$\checkmark$	positive	$i \psi_2\rangle$
$f_5$	$\checkmark$	$\times$	$\times$	negative	$-i \psi_4\rangle$
$f_6$	$\times$	$\checkmark$	$\times$	negative	$- \psi_4\rangle$
$f_7$	$\checkmark$	$\checkmark$	$\checkmark$	negative	$i \psi_4\rangle$
$f_8$	$\times$	$\times$	$\checkmark$	negative	$ \psi_4\rangle$

and its orthogonal state corresponding to equation (4) can be written as

$$\begin{aligned} (|\psi_4\rangle) &= (|+1\rangle - |-1\rangle)(|H\rangle - i|V\rangle)/2 \\ &= (|+1\rangle - |-1\rangle)|R\rangle/\sqrt{2} \end{aligned} \quad (7)$$

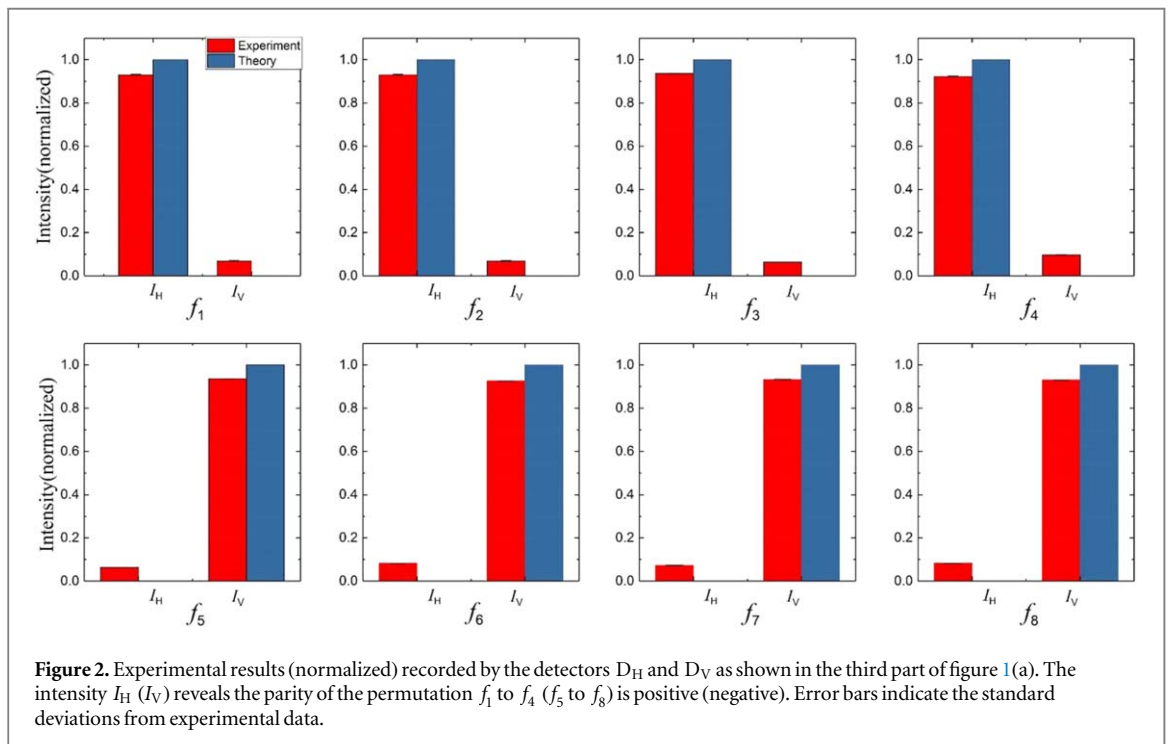
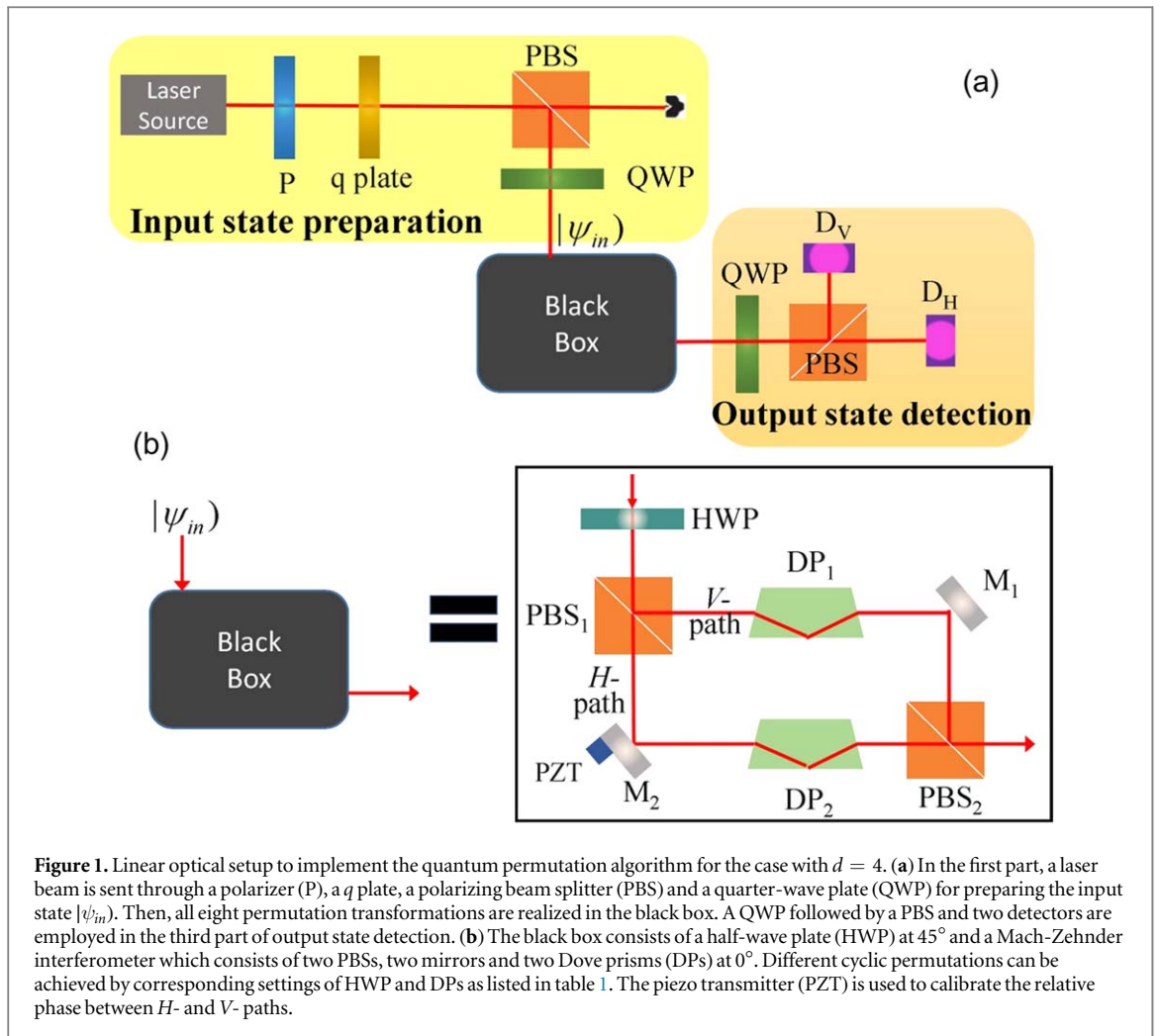
where  $|L\rangle$  and  $|R\rangle$  represent the left- and right-handed circular polarizations, respectively. Then all eight cyclic permutations and their resultant output states are listed in table 1, which shows the positive (negative) cyclic permutations map the input state  $|\psi_{in}\rangle$  onto  $|\psi_2\rangle$  ( $|\psi_4\rangle$ ) up to an overall phase factor.

### 3. Experiment and results

Figure 1(a) shows our experimental setup to demonstrate the permutation algorithm for the case with  $d = 4$ , which is comprised of three parts: the input state preparation, a black box and the output state detection. In the first part, a laser pulse emitted from the He-Ne laser source ( $\lambda = 632.8$  nm) with zero OAM is sent through a polarizer (P) that sets the polarization of the field horizontal, and then the state can be expanded as  $|\ell = 0, H\rangle = |0\rangle(|L\rangle + |R\rangle)/\sqrt{2}$ . Next, a voltage-controlled  $q$  plate [34] with a dimensionless parameter  $q = 0.5$  can conveniently transform the OAM and polarization of the beam into  $(|\ell = +1, R\rangle + |\ell = -1, L\rangle)/\sqrt{2}$  [18]. Then the vertical component reflected from a polarizing beam splitter (PBS) would be  $-i(|+1\rangle - |-1\rangle)|V\rangle/\sqrt{2}$ . Finally, a quarter-wave plate (QWP) at  $45^\circ$  transforms the polarization of the light into left-handed circular and yields the input state  $|\psi_{in}\rangle$  in equation (6), which is then sent into the black box.

The black box is composed of a half-wave plate (HWP) and a Mach-Zehnder interferometer, containing two PBSs 1 and 2, two mirrors ( $M_1$  and  $M_2$ ) and two Dove prisms (DP<sub>1</sub> and DP<sub>2</sub>), as shown in figure 1(b). The HWP at  $45^\circ$  interchanges  $H$  and  $V$  polarizations, while a mirror or a DP at  $0^\circ$  is used to flip the signs of the OAM modes (e.g.  $\ell = +1 \rightarrow -1$  or  $\ell = -1 \rightarrow +1$ ). Thus, all eight cyclic permutations can be realized by removing or adding the HWP and/or DPs (see table 1). For the purpose of illustration we take the realization of  $f_4$  operation for instance, which requires the existence of the HWP and DP<sub>2</sub>. First, the HWP transforms the input  $|\psi_{in}\rangle$  into  $(|+1\rangle - |-1\rangle)(|V\rangle + i|H\rangle)/2$ . Then after the PBS<sub>1</sub> in the interferometer, the light beam is divided into two orthogonal copies. The vertical component reflected from PBS<sub>1</sub> encounters the mirror  $M_1$  in the  $V$ -path that flips the signs of its OAM modes, while the horizontal component transmitted through PBS<sub>1</sub> into the  $H$ -path gets reflected twice by  $M_2$  and DP<sub>2</sub>, leading to its OAM modes unchanged. Finally, these two beams with orthogonal polarizations are recombined at the PBS<sub>2</sub> into the same path, and we obtain the output state  $i(|+1\rangle - |-1\rangle)(|H\rangle + i|V\rangle)/2$ , i.e.,  $i|\psi_2\rangle$ , indeed in agreement with theoretical predictions. With similar analysis, we list concrete settings to implement all permutation transformations in table 1.

Table 1 shows the output states from positive (negative) permutation operations are equivalent to the state in equation (6)–(7). Comparing equations (6) and (7) we conclude the final states output from different permutations with distinct parity have the same OAM modes but orthogonal polarizations, which in turn enables to experimentally determine the parity of a certain black box only by measuring the polarization as shown in the third part of figure 1(a). A QWP at  $45^\circ$  transforms the left- (right-) handed circular polarization of the output light into horizontal (vertical), and two power detectors  $D_H$  and  $D_V$  at the  $H$  and  $V$  ports of the following PBS record the light's intensity as  $I_H$  and  $I_V$ , respectively. In theory the results  $I_H = 1$  and  $I_V = 0$  (normalized) reveal the corresponding permutations are positive, while  $I_H = 0$  and  $I_V = 1$  indicate the negative parity. Figure 2 shows normalized intensities recorded by the detectors  $D_H$  and  $D_V$  for each of the eight cyclic permutations. Theoretically, the output  $I_H$  ( $I_V$ ) indicating the parity of positive (negative) permutations should



be 1. In our experimental results, the outcomes for  $f_1$  to  $f_4$  are  $I_H = 93.0 \pm 0.2\%$ ,  $93.1 \pm 0.3\%$ ,  $93.6 \pm 0.2\%$  and  $93.3 \pm 0.2\%$ , respectively, indicating the positive parity of them; while for  $f_5$  to  $f_8$  the outcomes  $I_V = 93.7 \pm 0.1\%$ ,  $92.6 \pm 0.1\%$ ,  $93.2 \pm 0.2\%$  and  $92.9 \pm 0.1\%$  determine their parity to be negative.

These qualified consequences that coincide with previous predictions come from the stability and robustness of our constructed classical wave system. For example, the Mach-Zehnder interferometer we establish is able to be stable for several hours, which is long enough for the process of data collection. In addition, to implement each permutation transformation precisely, the voltage of a piezo transmitter (PZT) mounted on  $M_2$  can be adjusted for calibrating the optical path difference between  $H$ - and  $V$ -paths that would be affected by adding or removing the Dove prism. The experimental errors are mainly attributed to the imperfection of optical devices, such as the inaccuracies of the  $q$  plate or HWP (QWP) setting angles, or the flaws in the polarizers and DPs. Thus, our measured outcomes are believed to approach the ideal results by a further improvement in experimental settings and operations.

#### 4. Discussions on higher-dimensional cases

The above discussions only focus on the permutation algorithm for the case with  $d = 4$ , and we can extend this classical scheme to higher-dimensional cases with the aid of previous investigations [30]. Compared with some previous quantum schemes [28, 29], our extended proposal takes full advantage of the high-dimensional properties of the OAM space to encode the required input state [32], and each cyclic permutation can be performed straightforwardly without constructing multi-qubit gates (e.g. Toffoli gate) [26]. Besides, the measurement and analysis of the outcomes are also easier to implement. Here we study the case with  $d = 8$  to illustrate how to realize larger-scale quantum permutation algorithms by expanding the superposition states of light's OAM modes.

Similar to equation (5), we utilize four OAM modes (e.g.  $\ell = -2, -1, 0, +1$ ) and polarization to represent eight basis states of a qudit ( $d = 8$ )

$$\begin{aligned} |-2, H\rangle &\rightarrow |1\rangle, |-2, V\rangle \rightarrow |2\rangle, |-1, H\rangle \rightarrow |3\rangle, |-1, V\rangle \rightarrow |4\rangle, \\ |0, H\rangle &\rightarrow |5\rangle, |0, V\rangle \rightarrow |6\rangle, |+1, H\rangle \rightarrow |7\rangle, |+1, V\rangle \rightarrow |8\rangle \end{aligned} \quad (8)$$

On this basis, the detailed experimental setup to demonstrate the permutation algorithm for the case with  $d = 8$  is presented in figure 3(a), which also consists of three parts similar to figure 1(a): the input state preparation, a black box and the output detection.

The input state is prepared in the first part similar to that in figure 1(a), in which a polarizer (P) and a QWP at  $45^\circ$  are kept to set the polarization left-handed circular and the  $q$  plate is replaced by a spatial light modulator (SLM) with a computer-generated hologram to transform the OAM modes as

$$|\psi_{in}\rangle = (|-2\rangle + i|-1\rangle - |0\rangle - i|1\rangle)(|H\rangle + i|V\rangle)/2\sqrt{2} = (1, i, i, -1, -1, -i, -i, 1)^T/2\sqrt{2}, \quad (9)$$

which then enters a black box.

Next, all 16 cyclic permutation operations can be realized in the black box by manipulating the OAM and polarization DOFs of the input light beam. Theoretically, the OAM modes of the output states corresponding to those 8 positive cyclic permutations are all in the superposition form

$$|\psi_2\rangle_{\text{OAM}} = (|-2\rangle + i|-1\rangle - |0\rangle - i|1\rangle)/2, \quad (10)$$

while other 8 negative cyclic permutation operations all result in the OAM mode as

$$|\psi_4\rangle_{\text{OAM}} = (|-2\rangle - i|-1\rangle - |0\rangle + i|1\rangle)/2. \quad (11)$$

To experimentally demonstrate these permutations, we still construct an interferometer in the black box as shown on the left hand side of figure 3(b). Unlike the use of Dove prisms to transform OAM modes in figure 1(b), here we introduce two modules  $f_H$  and  $f_V$  located in the  $H$ - and  $V$ -path separately to achieve desired manipulations of the light's OAM. The modules  $f_H$  and  $f_V$  can be chosen from the required mapping operations  $f_m^+/f_m^-$  ( $m = 0, 1, 2, 3$ ) as proposed in [30], which are able to rearrange the orders of the four OAM modes  $\{-2, -1, 0, +1\}$  as

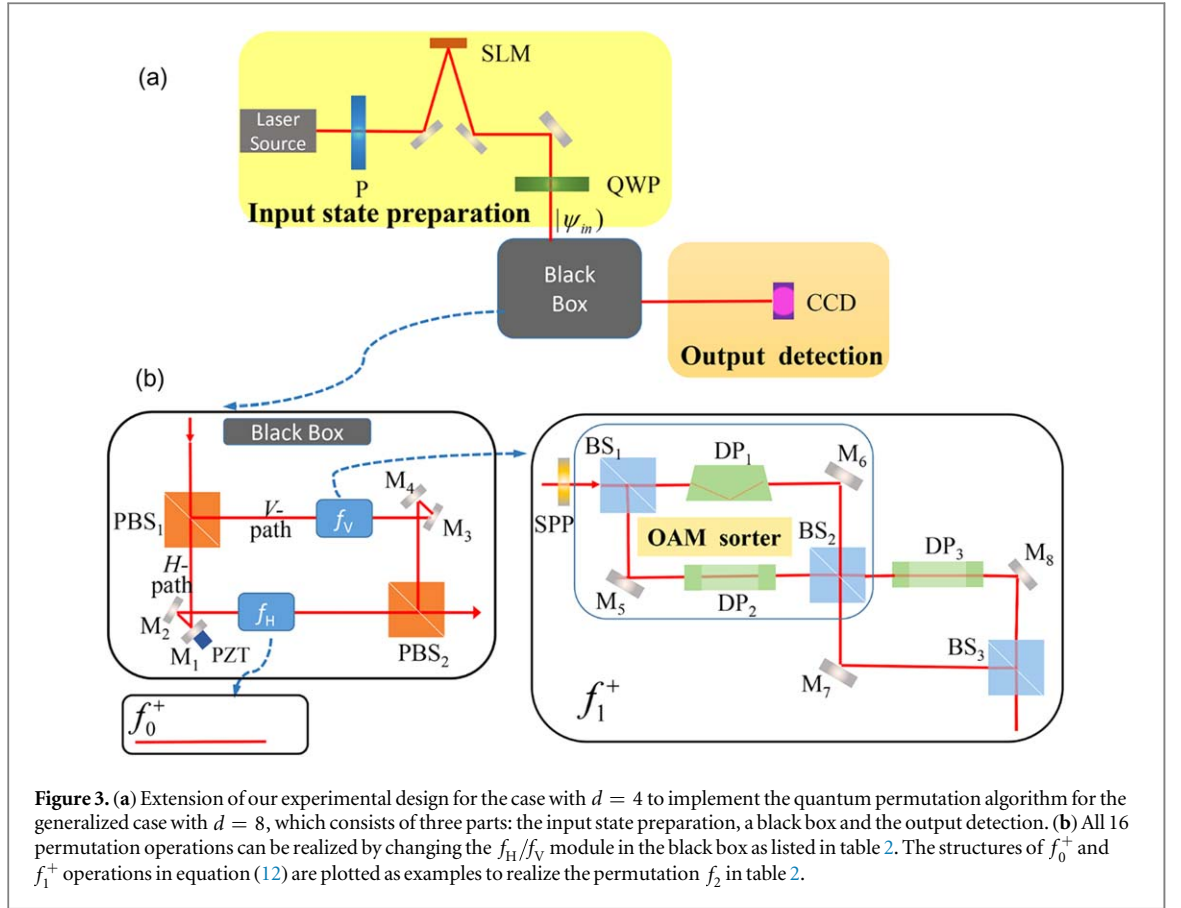


**Figure 3.** (a) Extension of our experimental design for the case with  $d = 4$  to implement the quantum permutation algorithm for the generalized case with  $d = 8$ , which consists of three parts: the input state preparation, a black box and the output detection. (b) All 16 permutation operations can be realized by changing the  $f_H/f_V$  module in the black box as listed in table 2. The structures of  $f_0^+$  and  $f_1^+$  operations in equation (12) are plotted as examples to realize the permutation  $f_2$  in table 2.

$$\begin{aligned}
 f_0^+ &= \begin{pmatrix} -2 & -1 & 0 & +1 \\ -2 & -1 & 0 & +1 \end{pmatrix}, f_1^+ = \begin{pmatrix} -2 & -1 & 0 & +1 \\ -1 & 0 & +1 & -2 \end{pmatrix}, \\
 f_2^+ &= \begin{pmatrix} -2 & -1 & 0 & +1 \\ 0 & +1 & -2 & -1 \end{pmatrix}, f_3^+ = \begin{pmatrix} -2 & -1 & 0 & +1 \\ +1 & -2 & -1 & 0 \end{pmatrix}, \\
 f_0^- &= \begin{pmatrix} -2 & -1 & 0 & +1 \\ -2 & +1 & 0 & -1 \end{pmatrix}, f_1^- = \begin{pmatrix} -2 & -1 & 0 & +1 \\ -1 & -2 & +1 & 0 \end{pmatrix}, \\
 f_2^- &= \begin{pmatrix} -2 & -1 & 0 & +1 \\ 0 & -1 & -2 & +1 \end{pmatrix}, f_3^- = \begin{pmatrix} -2 & -1 & 0 & +1 \\ +1 & 0 & -1 & -2 \end{pmatrix},
 \end{aligned} \tag{12}$$

Note the concrete optical designs for these operations  $f_m^+/f_m^-$  have been pointed out in [30] in detail, and here the structures of  $f_0^+$  and  $f_1^+$  are shown in figure 3(b) as examples. Besides, the two mirrors  $M_1$  and  $M_2$  ( $M_3$  and  $M_4$ ) in the  $H$  ( $V$ )-path are used to keep the signs of the OAM modes unchanged.

For example, to demonstrate the positive cyclic permutation  $f_2$  for  $d = 8$ , we choose the module  $f_H$  in the black box to be the operation  $f_0^+$  and  $f_V$  to be  $f_1^+$  as shown in figure 3(b). Here, the operation  $f_0^+$  is just the identity operation, while  $f_1^+$  is constructed from one spiral phase plate (SPP) followed by two cascaded interferometers. First, the four OAM modes in the  $V$ -polarization component of the input  $|\psi_{in}\rangle$  in equation (9) are added by  $\Delta\ell = +1$  through the SPP, i.e.  $i(|-2\rangle + i|-1\rangle - |0\rangle - i|1\rangle)|V\rangle \rightarrow i(|-1\rangle + i|0\rangle - |1\rangle - i|2\rangle)|V\rangle$ . Then, the interferometer composed of two beam splitters ( $BS_1$  and  $BS_2$ ), two Dove prisms ( $DP_1$  and  $DP_2$ ) and two mirrors ( $M_5$  and  $M_6$ ) acts as a typical OAM sorter [35], which reflects components with odd OAMs ( $i(|-1\rangle - |1\rangle)|V\rangle$ ) and transmit components with even OAMs ( $(-|0\rangle + |2\rangle)|V\rangle$ ) into the lower and upper arm of the next interferometer, respectively. Next, the sign of the even OAMs are inverted by a Dove prism ( $DP_3$ ) as  $(-|0\rangle + |2\rangle)|V\rangle \rightarrow (-|0\rangle + |-2\rangle)|V\rangle$ , which is recombined with those odd OAMs through  $BS_3$ . Finally, this vertical polarization component ( $(|-2\rangle + i|-1\rangle - |0\rangle - i|1\rangle)|V\rangle$ ) obtained from the  $f_1^+$  operation and the horizontal component ( $(|-2\rangle + i|-1\rangle - |0\rangle - i|1\rangle)|V\rangle$ ) from the  $f_0^+$  operation are recombined at the  $PBS_2$  into the output state as

$$|\psi_{out}\rangle_{f_2} = (|-2\rangle + i|-1\rangle - |0\rangle - i|1\rangle)(|H\rangle + |V\rangle)/2\sqrt{2}, \tag{13}$$

**Table 2.** Implementations and output states of 16 different permutation transformations for the case with  $d = 8$ . For each permutation, the modules  $f_H$  and  $f_V$  in the black box are chosen from the functions in (12) as required.

permutation operation	$f_H$	$f_V$	parity	output state	
				OAM	polarization
$f_1$	$f_0^+$	$f_0^+$	positive	$ \psi_2\rangle_{\text{OAM}}$	$ H\rangle + i V\rangle$
$f_2$	$f_0^+$	$f_1^+$	positive	$ \psi_2\rangle_{\text{OAM}}$	$ H\rangle +  V\rangle$
$f_3$	$f_1^+$	$f_1^+$	positive	$ \psi_2\rangle_{\text{OAM}}$	$-i H\rangle +  V\rangle$
$f_4$	$f_1^+$	$f_2^+$	positive	$ \psi_2\rangle_{\text{OAM}}$	$-i H\rangle - i V\rangle$
$f_5$	$f_2^+$	$f_2^+$	positive	$ \psi_2\rangle_{\text{OAM}}$	$- H\rangle - i V\rangle$
$f_6$	$f_2^+$	$f_3^+$	positive	$ \psi_2\rangle_{\text{OAM}}$	$- H\rangle -  V\rangle$
$f_7$	$f_3^+$	$f_3^+$	positive	$ \psi_2\rangle_{\text{OAM}}$	$i H\rangle -  V\rangle$
$f_8$	$f_3^+$	$f_0^+$	positive	$ \psi_2\rangle_{\text{OAM}}$	$i H\rangle + i V\rangle$
$f_9$	$f_0^-$	$f_2^-$	negative	$ \psi_4\rangle_{\text{OAM}}$	$ H\rangle - i V\rangle$
$f_{10}$	$f_3^-$	$f_2^-$	negative	$ \psi_4\rangle_{\text{OAM}}$	$-i H\rangle - i V\rangle$
$f_{11}$	$f_3^-$	$f_1^-$	negative	$ \psi_4\rangle_{\text{OAM}}$	$-i H\rangle -  V\rangle$
$f_{12}$	$f_2^-$	$f_1^-$	negative	$ \psi_4\rangle_{\text{OAM}}$	$- H\rangle -  V\rangle$
$f_{13}$	$f_2^-$	$f_0^-$	negative	$ \psi_4\rangle_{\text{OAM}}$	$- H\rangle + i V\rangle$
$f_{14}$	$f_1^-$	$f_0^-$	negative	$ \psi_4\rangle_{\text{OAM}}$	$i H\rangle + i V\rangle$
$f_{15}$	$f_1^-$	$f_3^-$	negative	$ \psi_4\rangle_{\text{OAM}}$	$i H\rangle +  V\rangle$
$f_{16}$	$f_0^-$	$f_3^-$	negative	$ \psi_4\rangle_{\text{OAM}}$	$ H\rangle +  V\rangle$

which indeed agrees well with our predictions in equation (10). Besides, the optical structures and working principles of other functions in equation (12) have also been explained in detail in Ref. [30], and thus the demonstration for other permutation operations can be implemented by similar settings as listed in table 2.

Table 2 shows the OAM modes of output states from positive (negative) permutation operations are the same as equation (10)–(11). Since these two distinct spatial modes are orthogonal, identifying the OAM modes of output states is enough to determine the parity of corresponding implemented cyclic permutation. As shown in the third part of figure 3(a), we can detect the output pattern distribution by a charge coupled device (CCD) camera and exploit the feasible methods used in [30], i.e., directly observing the pattern or calculating the fidelities, to distinguish the parity of the black box.

Compared with the scheme proposed in Ref. [30], we have introduced another degree of freedom, i.e. polarization, as an efficient route to increasing the biggest  $d$  achievable and simplifying the experiment. In our work, to encode a  $d$ -dimensional state, only  $d/2$  different OAM modes of classical light are needed and then manipulated in the  $f_H$  and  $f_V$  modules in the interferometer (see figure 3(b)). Thus, it seems that the biggest  $d$  achievable is limited to the number of experimentally accessible OAM modes and that of the associated optical elements (e.g. OAM sorter, interferometers), which would scale with the dimension  $d$ , i.e. show an exponential growth with the corresponding qubit number in quantum experiments [26, 29]. In the present experiments, obtaining higher-order OAM modes of light with high efficiencies and qualities still remains challenging, and the typically explored OAM modes range over  $\ell \in [-5, +5]$  in the optical experiments [36, 37], or up to order  $\ell = \pm 10$  [38], which would limit the generalization to higher-dimensional situations. Besides, constructing multiple interferometers would be a challenge to stabilize in the laboratory, and the imperfections of all used optical elements need to be considered. These drawbacks further limit the biggest  $d$  realized in the experiment. Considering these factors, the biggest  $d$  that can be achieved in our scheme is between 20 to 30, approximately corresponding to the quantum implementation of a 4- or 5-qubit case.

Several methods can be taken into account to mitigate the growth of optical elements as  $d$  increases. First, introducing other degrees of freedom of light, e.g. path or frequency, could contribute to encoding information [38, 39] and realizing larger-cycle rotations [40]. Second, the design of multiple interferometers is likely to be further optimized. For example, the OAM sorter used for manipulating different OAM modes in figure 3(b) is part of cascaded interferometers, and thus more efficient and economical alternatives could be considered for handling higher-dimensional cases [41, 42]. Third, the imperfections of optical components could be improved technically. For instance, placing the experimental elements as compact as possible with a soft buffer or in closed spaces can enable the interferometers more stable [28, 37]. These methods can be combined together for simplifications and improvements of the experiment.

## 5. Conclusions

We have experimentally realized the quantum permutation algorithm with an easy-handling optical setup. All eight cyclic permutation transformations have been completed by using the OAM and polarization DOFs of classical light beams, and their parity can be distinguished directly by simply detecting the polarization of the output states. Our results have shown that a total classical scheme can be used as an alternative to certain quantum systems for specific purposes, which is technically simple to realize and robust against disturbance. Also, we have discussed the theoretical extension to the case  $d = 8$  using four OAM modes. However, the generalization of our scheme to the cases with higher-dimensional state spaces would be limited by the number of experimentally accessible OAM modes and that of the associated optical elements, the complexity of constructing multiple interferometers in practice, and the imperfections of all used optical components. Considering these shortcomings, we have proposed feasible methods for simplifications and improvements of the experiment. Moreover, despite these limitations, such a designed optical set-up exploiting the OAM and polarization of classical light is well suited for in-principle verifications for specific small-scale linear optical quantum-information processing. Still, technique efforts need to be undertaken to make these focused permutation operations potential for extensive applications, such as some related high-dimensional quantum protocols [43, 44].

## Acknowledgments

This work was supported by the National key R & D Program of China under Grant No. 2017YFA0303800 and the National Natural Science Foundation of China (Grant No. 11574031 and 61421001).

## ORCID iDs

Shihao Zhang  <https://orcid.org/0000-0001-7725-4779>

Xiangdong Zhang  <https://orcid.org/0000-0002-7725-8814>

## References

- [1] Montanaro A 2016 Quantum algorithms: an overview npj *Quantum Information* **2** 15023
- [2] Harrow A W and Montanaro A 2017 Quantum computational supremacy *Nature* **549** 203
- [3] Ladd T D, Jelezko F, Laflamme R, Nakamura Y, Monroe C and O'Brien J L 2010 Quantum computers *Nature* **464** 45
- [4] Tame M, Prevedel R, Paternostro M, Böhi P, Kim M and Zeilinger A 2007 Experimental realization of deutsch's algorithm in a one-way quantum computer *Phys. Rev. Lett.* **98** 140501
- [5] Debnath S, Linke N M, Figgatt C, Landsman K A, Wright K and Monroe C 2016 Demonstration of a small programmable quantum computer with atomic qubits *Nature* **536** 63
- [6] Walther P, Resch K J, Rudolph T, Schenck E, Weinfurter H, Vedral V, Aspelmeyer M and Zeilinger A 2005 Experimental one-way quantum computing *Nature* **434** 169–176
- [7] Figgatt C, Maslov D, Landsman K A, Linke N M, Debnath S and Monroe C 2017 Complete 3-qubit grover search on a programmable quantum computer *Nature Communications* **8** 1918
- [8] Lu C-Y, Browne D E, Yang T and Pan J-W 2007 Demonstration of a compiled version of Shor's quantum factoring algorithm using photonic qubits *Phys. Rev. Lett.* **99** 250504
- [9] Monz T, Nigg D, Martinez E A, Brandl M F, Schindler P, Rines R, Wang S X, Chuang I L and Blatt R 2016 Realization of a scalable shor algorithm *Science* **351** 1068–1070
- [10] Cai X-D, Weedbrook C, Su Z-E, Chen M-C, Gu M, Zhu M-J, Li L, Liu N-L, Lu C-Y and Pan J-W 2013 Experimental quantum computing to solve systems of linear equations *Phys. Rev. Lett.* **110** 230501
- [11] Barz S, Kassal I, Ringbauer M, Lipp Y O, Dakić B, Aspuru-Guzik A and Walther P 2014 A two-qubit photonic quantum processor and its application to solving systems of linear equations *Sci. Rep.* **4** 6115
- [12] Preskill J 2018 Quantum computing in the NISQ era and beyond *Arxiv Preprint ArXiv* **1801** 00862
- [13] Karimi E, Leach J, Slussarenko S, Piccirillo B, Marrucci L, Chen L, She W, Franke-Arnold S, Padgett M J and Santamato E 2010 Spin-orbit hybrid entanglement of photons and quantum contextuality *Phys. Rev. A* **82** 022115
- [14] Gabriel C, Aiello A, Zhong W, Euser T, Joly N, Banzer P, Förtsch M, Elser D, Andersen U L and Marquardt C 2011 Entangling different degrees of freedom by quadrature squeezing cylindrically polarized modes *Phys. Rev. Lett.* **106** 060502
- [15] Li T, Zhang X, Zeng Q, Wang B and Zhang X 2018 Experimental simulation of monogamy relation between contextuality and nonlocality in classical light *Opt. Express* **26** 11959–11975
- [16] Perez-Garcia B, Francis J, McLaren M, Hernandez-Aranda R I, Forbes A and Konrad T 2015 Quantum computation with classical light: The deutsch algorithm *Physics Letters A* **379** 1675–1680
- [17] Perez-Garcia B, McLaren M, Goyal S K, Hernandez-Aranda R I, Forbes A and Konrad T 2016 Quantum computation with classical light: Implementation of the deutsch-jozsa algorithm *Physics Letters A* **380** 1925–1931
- [18] Goyal S K, Roux F S, Forbes A and Konrad T 2013 Implementing quantum walks using orbital angular momentum of classical light *Phys. Rev. Lett.* **110** 263602
- [19] Goyal S K, Roux F S, Forbes A and Konrad T 2015 Implementation of multidimensional quantum walks using linear optics and classical light *Phys. Rev. A* **92** 040302

- [20] Bhattacharya N, Hb V L V D H and Spreuw R J 2002 Implementation of quantum search algorithm using classical fourier optics *Phys. Rev. Lett.* **88** 137901
- [21] Zhang W, Cheng K, Wu C, Wang Y, Li H and Zhang X 2018 Implementing quantum search algorithm with metamaterials *Adv. Mater.* **30** 1703986
- [22] La Cour B R and Ott G E 2015 Signal-based classical emulation of a universal quantum computer *New J. Phys.* **17** 053017
- [23] La Cour B R and Ostrove C I 2017 Subspace projection method for unstructured searches with noisy quantum oracles using a signal-based quantum emulation device *Quantum Information Processing* **16** 7
- [24] Dogra S and Dorai K 2014 Determining the parity of a permutation using an experimental NMR qutrit *Physics Letters A* **378** 3452–6
- [25] Gedik Z, Silva I A, Çakmak B, Karpat G, Vidoto E L G, Soares-Pinto D d O and Fanchini F 2015 Computational speed-up with a single qudit *Sci. Rep.* **5** 14671
- [26] Yalçınkaya I and Gedik Z 2017 Optimization and experimental realization of the quantum permutation algorithm *Phys. Rev. A* **96** 062339
- [27] Dai K, Zhao P, Li M, Tan X, Yu H and Yu Y 2018 Demonstration of quantum permutation parity determine algorithm in a superconducting qutrit *Chin. Phys. B* **27** 060305
- [28] Wang F, Wang Y, Liu R, Chen D, Zhang P, Gao H and Li F 2015 Demonstration of quantum permutation algorithm with a single photon ququart *Sci. Rep.* **5** 10995
- [29] Zhan X, Li J, Qin H, Bian Z-h and Xue P 2015 Linear optical demonstration of quantum speed-up with a single qudit *Opt. Express* **23** 18422–18427
- [30] Chen D-X, Liu R-F, Zhang P, Wang Y-L, Li H-R, Gao H and Li F-L 2017 Realization of quantum permutation algorithm in high dimensional hilbert space *Chin. Phys. B* **26** 060305
- [31] Allen L, Beijersbergen M W, Spreuw R and Woerdman J 1992 Orbital angular momentum of light and the transformation of laguerre-gaussian laser modes *Phys. Rev. A* **45** 8185
- [32] Yao A M and Padgett M J 2011 Orbital angular momentum: origins, behavior and applications *Advances in Optics and Photonics* **3** 161–204
- [33] Song X, Sun Y, Li P, Qin H and Zhang X 2015 Bell's measure and implementing quantum Fourier transform with orbital angular momentum of classical light *Sci. Rep.* **5** 14113
- [34] Marrucci L, Manzo C and Paparo D 2006 Optical spin-to-orbital angular momentum conversion in inhomogeneous anisotropic media *Phys. Rev. Lett.* **96** 163905
- [35] Leach J, Padgett M J, Barnett S M, Franke-Arnold S and Courtial J 2002 Measuring the orbital angular momentum of a single photon *Phys. Rev. Lett.* **88** 257901
- [36] Ndagano B, Perez-Garcia B, Roux F S, McLaren M, Rosales-Guzman C, Zhang Y, Mouane O, Hernandez-Aranda R I, Konrad T and Forbes A 2017 Characterizing quantum channels with non-separable states of classical light *Nat. Phys.* **13** 397
- [37] Li P, Zhang S and Zhang X 2018 Classically high-dimensional correlation: simulation of high-dimensional entanglement *Opt. Express* **26** 31413–31429
- [38] Fickler R, Lapkiewicz R, Huber M, Lavery M P, Padgett M J and Zeilinger A 2014 Interface between path and orbital angular momentum entanglement for high-dimensional photonic quantum information *Nat. Commun.* **5** 4502
- [39] Hu H, Da Ros F, Pu M, Ye F, Ingerslev K, da Silva E P, Nooruzzaman M, Amma Y, Sasaki Y and Mizuno T 2018 Single-source chip-based frequency comb enabling extreme parallel data transmission *Nat. Photon.* **12** 469
- [40] Krenn M, Malik M, Fickler R, Lapkiewicz R and Zeilinger A 2016 Automated search for new quantum experiments *Phys. Rev. Lett.* **116** 090405
- [41] Berkhout G C, Lavery M P, Courtial J, Beijersbergen M W and Padgett M J 2010 Efficient sorting of orbital angular momentum states of light *Phys. Rev. Lett.* **105** 153601
- [42] Mirhosseini M, Malik M, Shi Z and Boyd R W 2013 Efficient separation of the orbital angular momentum eigenstates of light *Nat. Commun.* **4** 2781
- [43] Araújo M, Costa F and Brukner Č 2014 Computational advantage from quantum-controlled ordering of gates *Phys. Rev. Lett.* **113** 250402
- [44] Tavakoli A, Herbauts I, Żukowski M and Bourennane M 2015 Secret sharing with a single d-level quantum system *Phys. Rev. A* **92** 030302